ChemPubSoc Europe

DOI: 10.1002/cctc.201600843

CHEMCATCHEM Full Papers

A Doubly Biomimetic Synthetic Transformation: Catalytic Decarbonylation and Halogenation at Room Temperature by Vanadium Pentoxide

Sujoy Rana, Bhawana Pandey, Aniruddha Dey, Rameezul Haque, Gopalan Rajaraman,* and Debabrata Maiti*[a]

The halogenation of the C–H bond by metal-oxo-peroxo species and the decarbonylation of aldehydes by metal-peroxo species are performed routinely in biological systems. However, metal-mediated decarbonylative halogenation is unknown in nature. In this work, we have shown that widely available V_2O_5 and $VO(acac)_2$ (acac = acetylacetonate) can catalyze decarbonylative halogenation through the generation of an intermediate vanadium-oxo-peroxo species, which was characterized by using ^{51}V NMR, UV/Vis, and resonance Raman spectroscopy. Further detection of formic acid from the reaction mixture confirmed the biomimetic aspects of decarbonylative halogenation. A detailed experimental and DFT study indicated a concerted mechanism for this decarbonylative halogenation performed under simple and mild reaction conditions.

Introduction

Vanadium haloperoxidases (V-HPO) are involved in the halogenation of more than 4500 natural products. The reaction of H_2O_2 with the vanadium center in V-HPO results in the formation of a vanadium-oxo-peroxo species.[1] A subsequent halide attack forms a vanadium oxyhalide intermediate, which is primarily responsible for the halogenation of several natural products (Scheme 1).[1c,2] The vanadium ion is oxidatively inert during the process and maintains its 5+ oxidation state throughout the catalytic cycle. Several synthetic complexes that include an array of ligands coordinated to V centers have been reported to serve as functional mimics of V-HPO.[1a] In Nature, deformylation is a common phenomenon. Cytochrome-P450, 14α-demethylase, and cyanobacterial aldehyde decarbonylase dependent enzymes perform deformylation reactions with the elimination of formate.[3] In these cases, both mono- and dinuclear heme-iron(III)-peroxo species have been proposed as plausible intermediates. Synthetic mononuclear nonheme $[Fe^{III}(TMC)(\eta^2\text{-}O_2)]^+$ (side-on peroxo; TMC = 1,4,7,10-tetramethyl-1,4,7,10-tetraazacyclododecane) can promote the deformylation of aldehydes by the elimination of formate (HCO_2^-).[4] However, the coalescence of both decarbonylation and halogenation into a single-step decarbonylative halogenation can be envisaged with the vanadium-oxo-peroxo species (Scheme 2).[5]

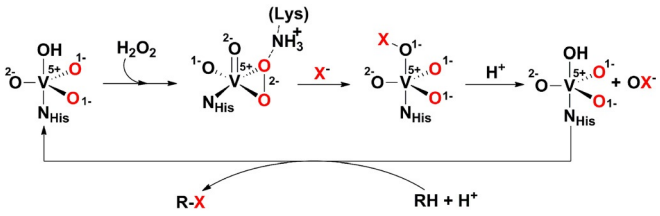

Scheme 1. Mechanistic action followed by V-HPO.

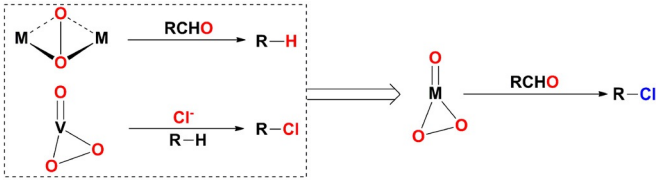

Scheme 2. Decarbonylation and halogenation reaction.

Results and Discussion

We envisioned that V_2O_5 (**1**) can produce vanadium-oxo-peroxo upon the addition of acid and H_2O_2 that will perform the decarbonylative halogenation in the presence of a halide and H_2O_2 (Scheme 3).

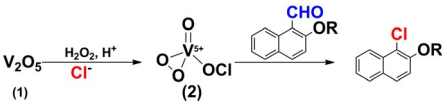

Scheme 3. Decarbonylative halogenation by V_2O_5.

[a] S. Rana, B. Pandey, A. Dey, R. Haque, Dr. G. Rajaraman, Dr. D. Maiti
Department of Chemistry
Indian Institute of Technology Bombay
Powai, Mumbai-400076 (India)
E-mail: gopalan.rajaraman@gmail.com
dmaiti@chem.iitb.ac.in

Supporting information for this article can be found under http://dx.doi.org/10.1002/cctc.201600843.

In addition, to realize this double-biomimetic reaction with V_2O_5, detailed experimental studies have been performed to elucidate the mechanism of this decarbonylative halogenation reaction. The commercial accessibility and the cost-effectiveness of V_2O_5 is expected to attract synthetic chemists to realize the full potential of these new strategies.

We started with the decarbonylative chlorination of 2-methoxynaphthaldehyde by V_2O_5 in the presence of KCl and H_2O_2. The desired 1-chloro-2-methoxynaphthalene was obtained in a good yield (Table 1, entry 1). In the absence of V_2O_5 with all

Table 1. Decarbonylative halogenation catalyzed by V_2O_5.

Entry	R—CHO → R—Cl (V_2O_5, KCl, H_2O_2)	Isolated yield [%]
1		52
2		50
3		10
4		30
5		20[a]

V_2O_5 (0.09 mmol), substrate (0.5 mmol), KCl (0.55 g, 7.5 mmol), H_2O_2 (330 μL, 3.25 mmol), acidic solution (prepared by the addition of HCl to water; 2 mL), citrate-phosphate buffer (2 mL), acetone (1 mL). [a] GC yield.

of the other reagents (e.g., KCl, H_2O_2) constant, the reaction was performed with 2-methoxy-1-naphthaldehyde. As expected, no trace of 1-chloro-2-methoxynaphthalene was obtained. Furthermore, exploration with 2-hydroxynaphthaldehyde also produced the expected 1-chloronaphthalen-2-ol (50%; Table 1, entry 2) by successful decarbonylation and chlorination.

The relatively electron-deficient substrate 6-bromo-2-methoxy-1-naphthaldehyde provided the corresponding decarbonylative halogenated product 6-bromo-1-chloro-2-methoxynaphthalene (30%; Table 1, entry 4). The decrease in the yield of the halogenated product is because of the presence of the electron-withdrawing bromide group at the 6-position. The α,β-unsaturated aldehyde 3,3-diphenylacrylaldehyde provided the corresponding decarbonylative halogenated product (2-chloroethene-1,1-diyl)dibenzene (10%) with benzophenone (15%) as a byproduct. Interestingly, if a more-electron-rich substrate was used the corresponding aromatic ring halogenation was observed. The electron-rich 2-aminobezaldehyde provided 2,4,6-tricloroaniline (20%; Table 1, entry 5). In this case, the aromatic ring was chlorinated after the formation of the decarbonylative halogenation product 2-chloroaniline because of the presence of an electron-rich amino group. The scope of the V_2O_5-catalyzed bromination reaction was explored with 2-methoxy-1-naphthaldehyde and 6-bromo-2-methoxy-1-naphthaldehyde in the presence of KBr and H_2O_2 under the standard reaction conditions. The decarbonylative bromination of 2-methoxy-1-naphthaldehyde provided the brominated product in 55% yield, whereas 6-bromo derivatives gave 40% of the desired product (Scheme 4).

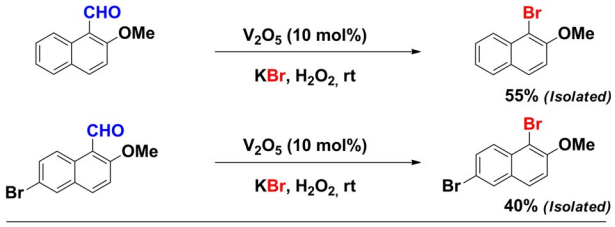

Scheme 4. Decarbonylative bromination by V_2O_5. V_2O_5 (0.09 mmol), KBr (0.55 g, 4.62 mmol), substrate (0.5 mmol), H_2O_2 (30%, 330 μL, 3.25 mmol), acidic water solution (H_2SO_4) in water (3 mL), citrate-phosphate buffer (2 mL), acetone (1 mL).

Interestingly, with bulky alkoxy groups (OR, R = allyl, propargyl, 2-chlorobenzyl) at the *ortho* position of 1-naphthaldehyde, trace amounts of halogenated products were obtained (Scheme 5). Such observations suggest the importance of the effective coordination of an alkoxy moiety to V during the decarbonylative halogenation reactions.

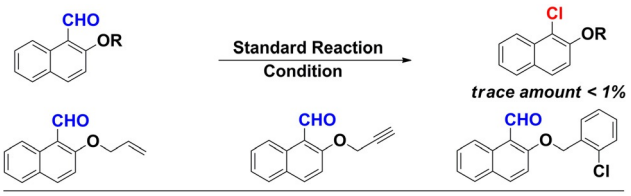

Scheme 5. Steric effect on decarbonylative halogenations.

UV/Vis spectra recorded in the absence of the exogenous substrate showed a band at $\lambda = 452$ nm ($\varepsilon = 391\ M^{-1}cm^{-1}$; Figure 1a), which indicated the formation of the red-colored vanadium-oxo-peroxo species (Figure 1a).[6] This characteristic absorption can be assigned as the peroxo to V^V charge transition band, which corresponds to $V^VO(O_2)$ species. Similar UV/Vis spectra for vanadium-oxo-peroxo species have been reported previously.[6] The same red solution of vanadium-oxo-peroxo species was further characterized by using ^{51}V NMR spectroscopy. The vanadium(V)-oxo-peroxo $VO(O_2)^+$ complex showed a sharp resonance at $\delta = -534.68$ ppm, which corroborated well with previous results (Figure 2a).[7]

Furthermore, the same red-colored solution of $VO(O_2)^+$ was characterized by using Raman spectroscopy. The Raman spectrum of $VO(O_2)^+$ showed the characteristic Raman shifts of $V–O_{peroxo}$ at $\tilde{\nu} = 550\ cm^{-1}$, O–O (side-on peroxo) at $\tilde{\nu} = 933\ cm^{-1}$, and the V=O bond at $\tilde{\nu} = 979\ cm^{-1}$ (Figure 3).[8]

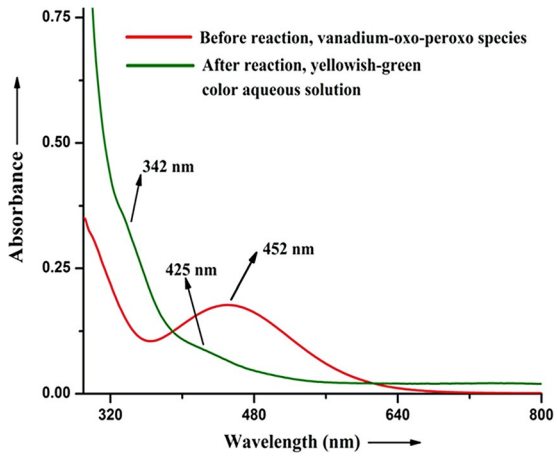

Figure 1. UV/Vis spectra recorded a) in the absence of organic substrate, b) in water after the addition of H_2O_2 and KCl to an acidic aqueous solution of V_2O_5 with the maximum at $\lambda = 452$ nm because of the formation of vanadium-oxo-peroxo species, and c) after the completion of the reaction in the presence of organic substrate, in which the yellowish-green color of the aqueous part is likely to be caused by VO_2^+.

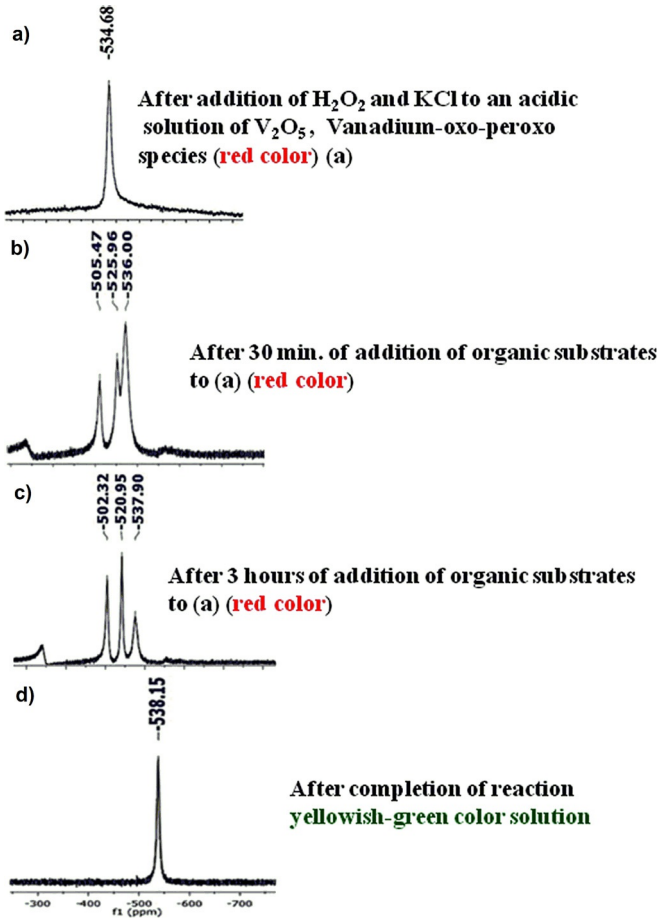

Figure 2. ^{51}V NMR spectra recorded during the course of decarbonylative halogenation reaction under the standard reaction protocol (in acidic aqueous medium) a) at the beginning of the reaction and in the absence of organic substrate (red-colored species), the vanadium oxo-peroxo species formed ($\delta = -534.68$ ppm), b) recorded after 30 min upon the addition of 2-methoxy-1-naphthaldehyde, c) recorded after 3 h, and d) after the completion of the reaction as a yellowish-green species.

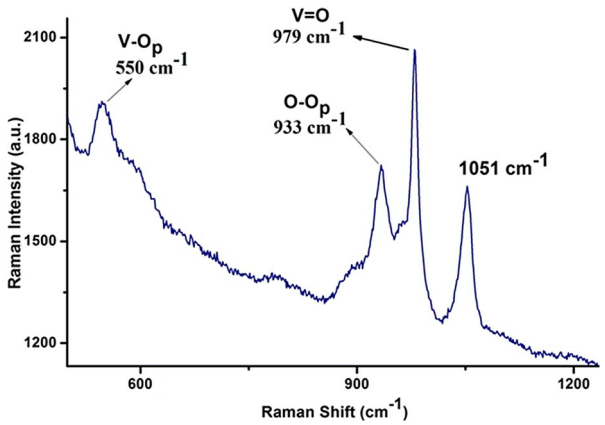

Figure 3. Raman spectrum of $V^VO(O_2)^+$, which shows the characteristic Raman shift of $V-O_{peroxo}$ at $\tilde{\nu} = 550$ cm^{-1}, O–O (side-on peroxo) at $\tilde{\nu} = 933$ cm^{-1}, and V=O at $\tilde{\nu} = 979$ cm^{-1}.

The FTIR spectrum of $V^VO(O_2)$ showed peaks that correspond to V=O stretching at $\tilde{\nu} = 987$ cm^{-1}, $O-O_P$ stretching at $\tilde{\nu} = 910$ cm^{-1}, and V–O stretching at $\tilde{\nu} = 615$ cm^{-1}.[6a,9]

The vanadium(V)-oxo-peroxo species can form $VO(O_2)(OCl)$ (**2**) easily in the presence of H_2O_2 and KCl in the absence of substrates to perform the decarbonylative halogenations reactions. If 2-methoxy-1-naphthaldehyde in acetone was added to the persistent red-colored solution (formed under the standard reaction conditions), which had a UV/Vis band at $\lambda = 452$ nm (Figure 1), the red solution turned green because of the formation of the decarbonylated halogenated product 1-chloro-2-methoxynaphthalene. The green-colored species displayed UV/Vis bands at $\lambda = 342$ (sh) and 425 nm (sh) (Figure 1).[10] The ^{51}V NMR spectrum of this species showed a sharp peak at $\delta = -538.15$ ppm, which could be attributed to the formation of a *cis*-dioxovanadium species ($V^VO_2^+$).[11] This green species turned to red-colored $V^VO(O_2)$ upon the addition of H_2O_2 to continue the catalytic cycle.

The ^{51}V NMR spectrum was recorded after the addition of 2-methoxy-1-naphthaldehyde in acetone to the $V^VO(O_2)(OH)^+$ solution. The spectrum showed some new upfield peaks at $\delta \approx -520$ and -502 ppm, which might be because of the substrate coordination to the vanadium-oxo-peroxo species. After the reaction, the green-colored solution showed an upfield peak at $\delta = -538.15$ ppm, which could be because of the formation of *cis*-dioxovanadium species (Figure 2d).[10d] The ^{51}V NMR spectra recorded at the beginning and at the end of the reaction showed chemical shifts at $\delta = -537.3$ and -538.1 ppm, respectively. These chemical shifts are particularly characteristic of the V^V oxidation state.[11] Therefore, the V^V oxidation state remains unaltered during the reaction.

In our attempt to achieve decarbonylative halogenation, the formation of formic acid was expected. Indeed the generation of formic acid was confirmed (yield = 50%) under the standard reaction conditions (Scheme 6). This observation, therefore, shows that our system mimics decarbonylation reactions by metal-peroxo complexes found in Nature.

Mechanistic investigations suggested that vanadium-oxo-peroxo species **2** was coordinated to an aldehyde substrate.

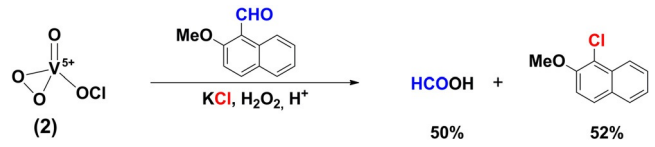

Scheme 6. Generation of formic acid.

The peroxo moiety reacted with the carbonyl center in **3** to produce **4** to provide the halogenated product in the presence of Cl^- and H_2O_2 by the generation of formic acid (Scheme 7). The active catalytic species **2** was regenerated in presence of H_2O_2 and Cl^-. Throughout the catalytic cycle, the V^V oxidation state was maintained similar to that of V-HPO enzymes.[1c,2e] As mononuclear vanadium-oxo-peroxo $V^VO(O_2)(OCl)$ (**2**) was responsible for the catalysis of the decarbonylative halogenation reaction, we aimed to generate a similar intermediate, which can be obtained from simple monomeric $V^{IV}O(acac)_2$ (**5**; acac = acetylacetonate) under the same reaction conditions as the V_2O_5-catalyzed decarbonylative chlorination.[6a,8c,12]

Interestingly, if we started from **5** we obtained 1-chloro-2-methoxy naphthalene from 2-methoxy-1-naphthaldehyde under the standard reaction conditions (Scheme 8). As expected, we observed the formation of a deep red solution after the addition of KCl/H_2O_2 that changed to green during the course of the reaction. These observations were further supported by the similar UV/Vis ($\lambda = 450$ nm) and ^{51}V NMR spectra ($\delta \approx -535$ ppm).[8c] The generation of formic acid was also confirmed during the decarbonylative halogenation reaction with **5**.

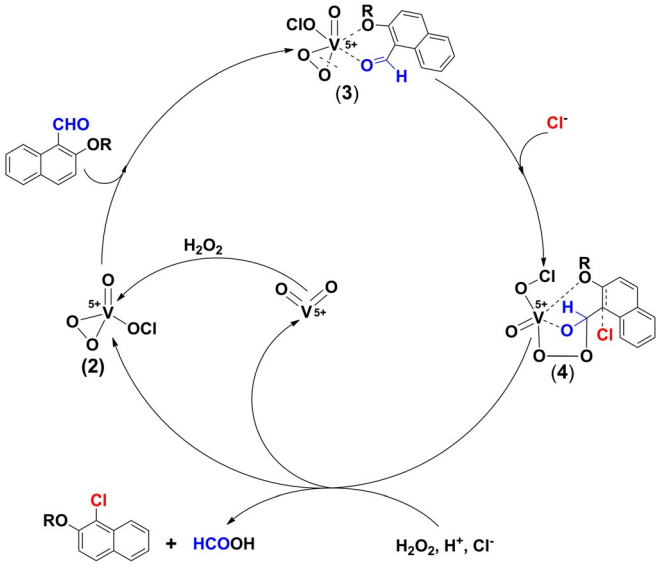

Scheme 7. Proposed mechanism based on experimental evidence.

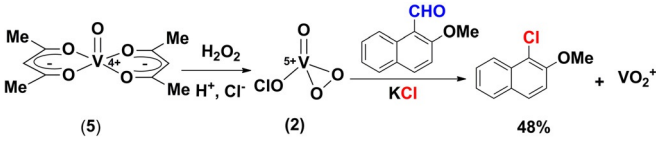

Scheme 8. Decarbonylative chlorination by $V^{IV}O(acac)_2$.

Insights in the mechanistic steps from DFT calculations

To understand the intricate steps in this reaction, we performed a DFT study to probe the mechanism. Based on our experimental observations, a mechanistic scheme was adapted for the DFT calculations (Scheme 9). We explored the energy

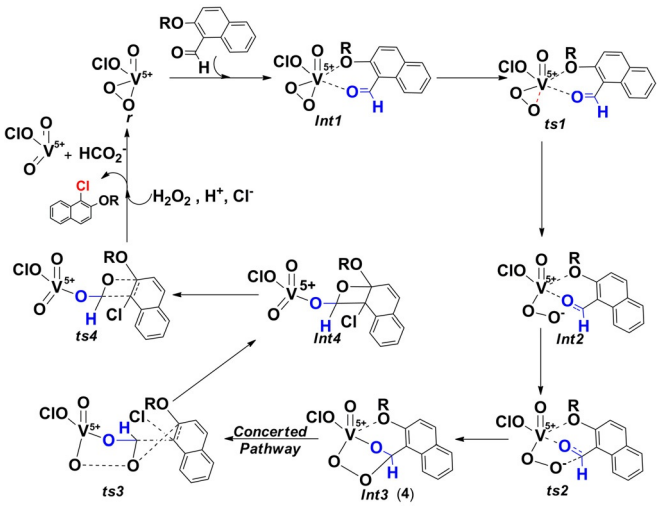

Scheme 9. Proposed mechanism for the decarbonylative halogenations based on DFT studies.

landscape for the interaction of aldehyde with vanadium-oxo-peroxo hydroxo $[V^VO(O_2)(OH)]$ species and with vanadium-oxo-peroxo hypochlorite species $[V^VO(O_2)(OCl)]$ (**2**). Our calculations revealed that the interaction of aldehyde with vanadium-oxo-peroxo hypochlorite species was more exothermic by 8 kJ mol^{-1} than the vanadium-oxo-peroxo hydroxo species. Thus we decided to begin our investigation with the vanadium-oxo-peroxo hypochlorite species **2**. Although vanadium hypobromites are known,[1c,9b,14] recent reports suggest the involvement of hypochlorite as the catalytically active species particularly for heme-iron systems.[15] This, along with the computed energetics, suggest vanadium hypochlorite as the starting species in our catalytic reaction. Additionally, this species has a high relevance to the active site of vanadium haloperoxidase.[16] The geometry around V was trigonal planar, and the V=O bond was calculated to be 1.580 Å. The other two peroxo O atoms were bonded symmetrically with bond length of 1.787 Å. The V–O(Cl) bond length was estimated to be 1.797 Å. In the next step, the ligand L (L = 2-methoxy napthaldehyde, Scheme 9) was assumed to coordinate to the vanadium-oxo-peroxo hypochlorite species. The optimized structure of this prereacting species is shown in Scheme 9. Energetically, this step was estimated to be exothermic in nature by −34.9 kJ mol^{-1}. This species, which has a literature precedent,[14b,16a] had a significant relevance to the active site of the vanadium haloperoxidase, and the only difference was the co-

ordination of the aldehyde O atoms instead of a N atom of an imidazole ring. Selected bond parameters of the optimized structures are given in Table S1.[8c]

The optimized structure revealed that the O atom of the –CHO group formed a strong coordination bond to the V (2.012 Å), and the O atom of the –OMe group coordinated weakly (3.111 Å) to the center. The V=O bond length was estimated to be 1.590 Å, and the peroxo O atoms were coordinated asymmetrically to the V atom (1.799 and 1.836 Å). The V–O(Cl) and O–Cl bond lengths were 1.825 and 1.706 Å, respectively. A significant difference in the structure here compared to the reactant species was the asymmetric nature of the peroxo group with one long and one short V–O bond. Significant σ/π-donation from the carbonyl O atom influenced the peroxo bonding as a clear π donation from only one of the O atoms (which possessed a shorter V–O distance) was visible (Figure 4). Another significant distinction was on the ligand moiety, in which the aldehyde C atom, C(1), developed a significant positive charge (Mulliken charge analysis revealed an increase from 0.89 in the free ligand to 1.22 in int2) upon coordination.

The coordination of the ligand, which induced asymmetry in the peroxo moiety, was the key to the next step, in which the longer V–O bond was expected to cleave. This was assumed to take place via ts1 (Figure 4) to lead to the formation of a V–O–O$^-$ species as an intermediate (int2; Figure 4).[8c] V–O bond cleavage was heterolytic consistent with the mechanism proposed for the vanadium haloperoxidases mimics.[14b,c,16a]

In ts1, the V–O bond elongated from 1.836 to 2.300 Å, and the other V–O bond of the peroxo moiety was shortened. The O–O bond length also shortened significantly as a greater electron density was available at the distal O atom. The calculated barrier height for this step was estimated to be 74.2 kJ mol^{-1} (Figure 4). The formation of the int2 species was slightly endothermic with respect to int1, however, from the reactant energy, it was still exothermic.

Thus the next logical step was the attack of the end-on peroxo species on the aldehyde C atom via ts2 (Figure 4).[8c]

The nucleophilic character of the end-on/side-on peroxo species with various metal ions was probed in detail. Particularly, the deformylation by the iron(III)-peroxo species indicated clearly that these species were nucleophilic.[17] Thus all these literature precedents support our mechanistic hypothesis. The attack of the distal O atom at the C atom led to the elongation of the O–O bond from 1.343 to 1.415 Å. The new O(2)–C(1) distances were estimated to be 1.900 Å, which shows a significant bonding interaction even in the transition state. The transition state showed a stronger interaction between the methoxy O atom with the V center (from 2.567 Å in int2 to 2.210 Å; Figure 4).[8c] The barrier height for this step was estimated to be 91.7 kJ mol^{-1} from int2, whereas on the reactant scale it was 63.3 kJ mol^{-1} (Figure 4).[8c]

In the next step, the formed O(2)–C(1) bond is completed (1.434 Å) to lead to int3 (Figure 4).[8c] This intermediate formation was exothermic by 82.6 kJ mol^{-1} from the reactant, which suggests the feasible formation of this species.

Incidentally, a five-coordinate hypochlorite that attacks the C atom was ruled out based on the following arguments: (i) the OCl$^-$ group was far away from the C(2) atom (4.986 Å), (ii) as per the experimental conditions, the solution contained a significant amount of chloride ions, which makes the external attack by a Cl$^-$ ion feasible, and (iii) a dissociative pathway in which O–Cl bond breaking first leads to the generation of Cl$^-$ species was unlikely as the bond-dissociation energy for the O–Cl bond was very large (+443.5 kJ mol^{-1}).

In the transition state, the new Cl–(C2) bond length was estimated to be 2.45 Å (Figure 4). Interestingly, the attack of the chloride ion at the C(2) position via this transition state was a concerted process in which the approach of the chloride ion triggered two structural changes: (i) at the transition state, the O–O bond breaks away (2.422 Å at ts3) and (ii) a new O(2)–C(3) bond was formed (1.443 Å at ts3). Furthermore, there was a slight elongation of the C(1)–C(2) bond (1.530 Å at ts3). At the transition state, steps (i) and (ii) were already completed, and step (iii) showed signs of progress towards the cleavage of the C(1)–C(2) bond. The intrinsic reaction coordinate (IRC) calculations confirmed this point, at 2.5 Å Cl–(C2),

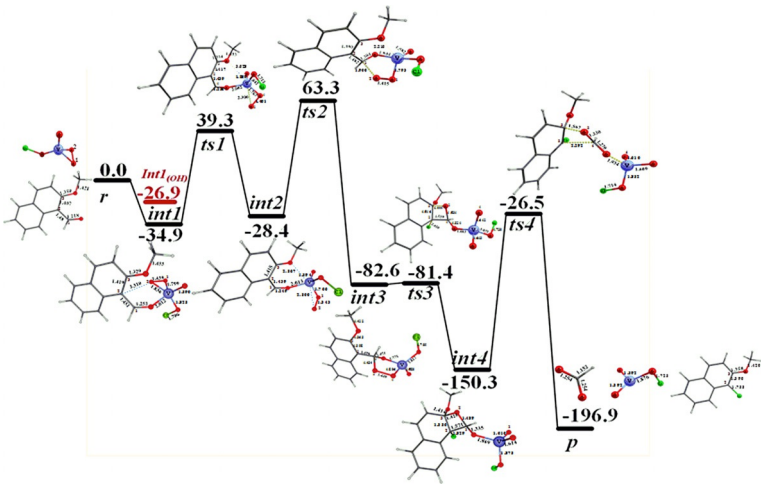

Figure 4. B3LYP computed energy (in solvent; ΔG in kJ mol^{-1}) profile diagram for the decarbonylative halogenations.

the peroxo bonds were not broken, however, at 2.45 Å Cl–(C2), the O–O bond was broken and the O(2)–C(3) bond was formed partially. Despite all these structural changes, the barrier height computed for this transition state was 1.2 kJ mol^{-1} from int3, which reveals a nearly barrierless process that leads to the formation of int4 (Figure 4).[8c]

In the next step the C(l)–(C2) bond was formed completely (1.829 Å), and the O(2)–C(3) bond strengthened further (1.425 Å). The formation of this intermediate was excessively exothermic in nature (−150.3 kJ mol^{-1} from the reactant). Notably, at this intermediate (int4), a constrained four-membered ring (C–C–C–O; Figure 4) existed, and in the next step this ring was expected to cleave via ts4 (Figure 4). The C(1)–C(2) and O(2)–C(3) bonds cleaved to result in the formation of formic acid and the decarbonylated halogenated product.

The C(1)–C(2) and O(2)–C(3) bond lengths were 2.292 and 1.567 Å, respectively. Although there was a significant kinetic barrier for this species from int4, from the reactant surface, it lay at 26.5 kJ mol^{-1}, which suggests the feasible formation of the product. The formation of the final product was a thermodynamic sink with a stabilization of −196.9 kJ mol^{-1}, and this energy gain was likely to ease the barrier heights required for the next catalytic cycle.[18] The potential-energy surface developed for the catalytic cycle studied is shown in Figure 4. The catalytic cycle was assumed to start from vanadium-oxo-peroxo hypochlorite species. This species was characterized by using spectroscopic methods. In the next step, the ligand was assumed to coordinate to this species to lead to the formation of [V(O)(O_2)(OCl)(L)] species. This step was computed to be exothermic, and the formation of this species was also witnessed in the experiments by variation in the ^{51}V NMR chemical shift. The ^{51}V NMR chemical shifts were associated qualitatively with the HOMO–LUMO gap, and such analysis is well supported by previous reports for several vanadyl complexes.[19] For species **2**, the HOMO–LUMO gap was computed to be 3.1 eV, which decreased drastically to 1.2 eV for int1, which suggests a significant shift in the ^{51}V NMR shift as observed in the experiments.[20]

The first transition state had a barrier height of 74.2 kJ mol^{-1}, and the second transition state had a much higher energy barrier (91.7 kJ mol^{-1}). These two transition states formed the key to the product formation, and the second step was rate limiting. Although the absolute barrier height of 91.7 kJ mol^{-1} seemed high, on a relative scale to the reactant, the peak energy was placed at 63.3 kJ mol^{-1}, that is, the energy gained upon ligand coordination eased the kinetic requirement. The large energy barrier computed also correlates with the experimental fact that the reactions were very slow and required a long time for completion (nearly 6–24 h).

The first transition state required significant energy as the strong V–O bond of the peroxo group needed to be broken. Apart from the strong σ-interaction, there was also significant π-donation from the peroxo group that enhanced the barrier height. A stronger π-interaction was correlated to the formal oxidation state of the V^V ions. For other transition metal ions that possess half-filled and more than half-filled orbitals, the breakup of the peroxo species was a facile step to lead to the formation of highly reactive end-on peroxo/superoxo species.[17a,c,21] Although the second transition state was electrostatically favorable as discussed earlier, a significant penalty in energy arose because of the structural distortion required to attain this transition state and the unfavorable orientation of the π*(C=O) orbital (Figure 4).[8c] The large exothermic gain upon reaching intermediate 3 made other steps feasible and facilitated a faster reaction. The ts3 was a concerted process in which several key structural alterations took place as confirmed by our IRC calculations. The approach of the chloride ion was essential to trigger a series of structural alterations.

Such a concerted step also correlated to the experimental observation that decarbonylative products are not detected in the reaction mixture. Without the addition of KCl, no product formation (decarbonylation, oxidation of aldehyde etc.) was detected, which thereby suggests the necessity of external stimuli to drive the reaction as revealed by ts3. Thus the proposed mechanism rationalizes all the experimental observations and suggests that this is the likely pathway through which the chlorination of aromatic compounds takes place. Among the species computed, only marginal changes in the V charge were noted (1.09 to 1.27; Table S2).[8c] This suggests that the 5+ oxidation state of V was maintained throughout the reaction. A recent ^{51}V NMR study on vanadium haloperoxidases suggests the presence of spectroscopically silent V^V during the catalytic cycle as revealed in our biomimetic models.[16b] The mechanism proposed has high relevance to biology particularly if vanadium haloperoxidase is found to halogenate thousands of natural products. Some of the key steps are likely to be common to both the enzymes and the biomimetic chemistry proposed in this work.

Conclusion

We have developed a decarbonylative halogenation procedure that starts with simple and readily available vanadium pentoxide. We have shown that a vanadium-oxo-peroxo species formed in situ is responsible for the decarbonylative halogenation reaction in the presence of chloride through the elimination of formate. The proposed mechanism of decarbonylative halogenation by vanadium-oxo-peroxo species based on our experimental findings is supported by the results of detailed DFT studies.

Experimental Section

General information

Isolated compounds were characterized by using ^{1}H and ^{13}C NMR spectroscopy and GC–MS. IR spectra were recorded by using a FTIR spectrometer, and the samples were prepared as KBr pellets. NMR spectra were recorded by using either a Bruker 400/500 MHz or on a Varian 300/400 MHz instrument. All ^{51}V NMR spectra were recorded in D_2O and reported in ppm relative to NH_4VO_3 (−571.5 ppm)[13].

Procedure A for decarbonylative chlorination

V_2O_5 (18 mol%, ≈17 mg) was taken in a 20 mL screw-capped reaction tube. Acidic aqueous solution (2 mL; 33 mL of concentrated HCl in 300 mL distilled water) was added followed by KCl (0.55 g, 7.5 mmol). Subsequently, the substrate (0.5 mmol) in acetone (1 mL) was added. Finally, 30% H_2O_2 (330 μL, 12 mmol) was added to the contents of the reaction tube, and the screw cap was closed and sealed with paraffin. The reaction tube was kept at RT with constant stirring. After 12 h, dichloromethane (50 mL) was added to the reaction mixture, and the organic component was extracted. The process was repeated, and the organics were combined and dried over Na_2SO_4 and concentrated under reduced pressure by using a rotary evaporator. The crude product was purified by column chromatography, and the yield of the isolated product was calculated with respect to the starting material used in the reaction.

Procedure B for decarbonylative bromination

V_2O_5 (18 mol%, ≈17 mg) was taken in a 20 mL screw-capped reaction tube. Acidic water (3 mL; 10–15 μL of concentrated H_2SO_4 in 3 mL of water) was added followed by citrate-phosphate buffer (2 mL). KBr (0.55 g, 4.62 mmol) was added to this resulting solution. Subsequently, substrate (0.5 mmol) in acetone (1 mL) was added. Finally, 30% H_2O_2 (330 μL) was added to the contents of the reaction tube, and the screw cap was closed and sealed with paraffin. The reaction tube was kept at RT with constant stirring. After 12 h, dichloromethane (50 mL) was added to the reaction mixture, and the organic component was extracted. The process was repeated, and the organics were combined and dried over Na_2SO_4 and concentrated under reduced pressure by using a rotary evaporator. The crude product was purified by column chromatography, and the yield of the isolated product was calculated with respect to the starting material used in the reaction.

Preparation of acidic water solution

In a 500 mL beaker, concentrated HCl (12 M, 33 mL, Merck Chemicals) was added to distilled water (300 mL) to form a dilute acid solution. Alternatively, H_2SO_4 (250 μL) was added to distilled water (10 mL) with stirring to make it homogeneous. Both acidic solutions were used for the decarbonylative halogenation reactions and the characterization of the reactive intermediates. We obtained similar observations by using both acidic solutions.

Sample preparation for ^{51}V NMR spectroscopy

D_2O (2 mL) was added to V_2O_5 (20 mg) in a vial followed by concentrated H_2SO_4 (40 μL). H_2O_2 (30%, 330 μL, 3.25 mmol) and KCl (0.55 g, 7.5 mmol) were added, and the mixture was stirred for 5–10 min before the NMR spectrum was recorded. A similar solution was prepared to which 2-methoxy-1-naphthaldehyde in acetone was added and stirred until the green color appeared. ^{51}V NMR spectra were recorded during reaction after 30 min and 3 h and after the completion of the reaction when the green color appeared.

Sample preparation for UV/Vis spectroscopy

Water (2 mL) was added to V_2O_5 (20 mg) in a 20 mL glass vial followed by H_2SO_4 (50 μL). H_2O_2 (30%, 330 μL, 3.25 mmol) and KCl (0.55 g, 7.5 mmol) were added to the solution. Then, citrate-phosphate buffer (2 mL) was added, and a UV/Vis spectrum was recorded from the resulting solution, which showed a band at $\lambda =$ 452 nm. Alternatively, H_2O (2 mL) and H_2SO_4 (40 μL) were added to V_2O_5 (20 mg) in a vial, and the mixture was stirred for 5 min. H_2O_2 (330 μL, 3.25 mmol) and KCl (0.55 g, 7.5 mmol) were added, and the mixture was stirred for 5 min. The resulting solution was used for UV/Vis spectrophotometry. The acid solution prepared from concentrated HCl in distilled water provides the same spectra of the vanadium-oxoperoxo complex.

Raman spectroscopy

We recorded resonance Raman spectra of the vanadium-oxo-peroxo species by using a confocal Raman microscope (alpha 300R, WITec, Germany). A frequency-doubled DPSS Nd:YAG laser of $\lambda = 532$ nm was used at a power of 5 mW to excite the vanadium-oxo-peroxo sample in mili-Q water in a constant flow through 1 mm flow-cell. The scattered light in the focal plane was collected through a 100 μm core multimode fiber as the pinhole. The spectra were collected at an integration time of 60 s by using a lens-based ultrahigh throughput spectrometer (UHTS300, 1800 grooves/mm grating) coupled to a back-illuminated charge-coupled device (CCD) camera (1024×128 pixels, ~2 cm^{-1} per CCD pixel).

Sample preparation for Raman spectroscopy

Water (2 mL) and H_2SO_4 (40 μL) were added to V_2O_5 (20 mg) in a 20 mL glass vial. Subsequently, H_2O_2 (30%, 330 μL, 3.25 mmol) and KCl (0.55 g, 7.5 mmol) were added to the solution, and it was stirred for 5–10 min. The spectrum of the resulting solution showed UV/Vis band at $\lambda = 452$ nm. The prepared solution was used for Raman spectroscopy.

Computational details

We used the Gaussian 09 suite of programs to perform all the calculations.[22] The geometry optimizations were performed with the B3LYP functional.[23] The B3LYP has a proven track record to predict the structures and energetics accurately for such metal-mediated catalytic reactions. The LACVP basis set that comprises LanL2DZ—Los Alamos effective core potential for V[24] and a 6–31G*[25] basis set for the other atoms (B-I) were employed for geometry optimization, and the optimized geometries were then used to perform single-point energy calculations using a TZVPP basis set (B-II) on all atoms.[26] The solvation energies were computed using the polarizable continuum model (PCM) solvation model, and acetonitrile was employed as the solvent.[27] Frequency calculations were performed on the optimized structures at B-I level to verify that they were minima on the potential-energy surface (PES) and to obtain free energy corrections. The quoted DFT energies were B3LYP solvation energies that incorporated zero-point energy corrections at the B-I level computed at 298.15 K, unless otherwise mentioned. The transition states were characterized by a single negative frequency that corresponds to the reaction coordinate and were verified by animating the frequency using visualization software such as Molden.[28]

Acknowledgements

This activity is supported by SERB-India (EMR/2015/000164). Financial support has been received from CSIR-India/UGC-India (fellowships to S.R. and B.P.). D.M. sincerely thanks Dr. Jyotishman Dasgupta (TIFR) and his group member Ms. Ankita Das for helping to conduct resonance Raman spectroscopy in his laboratory.

Keywords: biocatalysts · density functional calculations · halogenation · reaction mechanisms · vanadium

[1] a) F. H. Vaillancourt, E. Yeh, D. A. Vosburg, S. Garneau-Tsodikova, C. T. Walsh, *Chem. Rev.* **2006**, *106*, 3364 – 3378; b) D. G. Fujimori, C. T. Walsh, *Curr. Opin. Chem. Biol.* **2007**, *11*, 553 – 560; c) A. Butler, M. Sandy, *Nature* **2009**, *460*, 848 – 854; d) L. C. Blasiak, C. L. Drennan, *Acc. Chem. Res.* **2009**, *42*, 147 – 155.

[2] a) R. Wever, H. Plat, E. de Boer, *Biochim. Biophys. Acta Protein Struct. Mol. Enzymol.* **1985**, *830*, 181 – 186; b) J. Littlechild, E. Garcia Rodriguez, M. Isupov, *J. Inorg. Biochem.* **2009**, *103*, 617 – 621; c) A. Butler, J. N. Carter-Franklin, *Nat. Prod. Rep.* **2004**, *21*, 180 – 188; d) W. Hemrika, R. Renirie, S. Macedo-Ribeiro, A. Messerschmidt, R. Wever, *J. Biol. Chem.* **1999**, *274*, 23820 – 23827; e) V. Conte, A. Coletti, B. Floris, G. Licini, C. Zonta, *Coord. Chem. Rev.* **2011**, *255*, 2165 – 2177; f) A. Messerschmidt, R. Wever, *Proc. Natl. Acad. Sci. USA* **1996**, *93*, 392 – 396; g) J. Littlechild, E. Garcia-Rodriguez, *Coord. Chem. Rev.* **2003**, *237*, 65 – 76; h) M. Weyand, H. J. Hecht, M. Kieß, M. F. Liaud, H. Vilter, D. Schomburg, *J. Mol. Biol.* **1999**, *293*, 595 – 611.

[3] a) K. Sen, J. C. Hackett, *J. Phys. Chem. B* **2009**, *113*, 8170 – 8182; b) K. Sen, J. C. Hackett, *J. Am. Chem. Soc.* **2010**, *132*, 10293 – 10305; c) C. Krebs, J. M. Bollinger Jr., S. J. Booker, *Curr. Opin. Chem. Biol.* **2011**, *15*, 291 – 303; d) K. M. Henry, C. A. Townsend, *J. Am. Chem. Soc.* **2005**, *127*, 3724 – 3733; e) A. Schirmer, M. A. Rude, X. Li, E. Popova, S. B. del Cardayre, *Science* **2010**, *329*, 559 – 562; f) L. J. Rajakovich, H. Nørgaard, D. M. Warui, W.-c. Chang, N. Li, S. J. Booker, C. Krebs, J. M. Bollinger, M.-E. Pandelia, *J. Am. Chem. Soc.* **2015**, *137*, 11695 – 11709.

[4] a) J. Annaraj, Y. Suh, M. S. Seo, S. O. Kim, W. Nam, *Chem. Commun.* **2005**, 4529 – 4531; b) A. Shokri, L. J. Que, *J. Am. Chem. Soc.* **2015**, *137*, 7686 – 7691.

[5] S. Rana, R. Haque, S. Ganji, D. Maiti, *Inorg. Chem.* **2013**, *52*, 2927 – 2932.

[6] a) C. R. Waidmann, A. G. DiPasquale, J. M. Mayer, *Inorg. Chem.* **2010**, *49*, 2383 – 2391; b) M. Sivak, *Chem. Pap.* **1987**, *41*, 311 – 319; c) M. Sivák, P. Schwendt, *Transition Met. Chem.* **1989**, *14*, 273 – 276; d) H. Kelm, H. J. Kruger, *Angew. Chem. Int. Ed.* **2001**, *40*, 2344 – 2348; *Angew. Chem.* **2001**, *113*, 2406 – 2410; e) R. M. Tótaro, P. A. M. Williams, M. C. Apella, M. A. Blesa, E. J. Baran, *J. Chem. Soc. Dalton Trans.* **2000**, 4403 – 4406; f) A. Shaver, J. B. Ng, D. A. Hall, B. I. Posner, *Mol. Cell. Biochem.* **1995**, *153*, 5 – 15; g) A. B. P. Lever, H. B. Gray, *Acc. Chem. Res.* **1978**, *11*, 348 – 355.

[7] L. L. G. Justino, M. L. Ramos, F. Nogueira, A. Sobral, C. Geraldes, M. Kaupp, H. D. Burrows, C. Fiolhais, V. M. S. Gil, *Inorg. Chem.* **2008**, *47*, 7317 – 7326.

[8] a) J. E. Molinari, I. E. Wachs, *J. Am. Chem. Soc.* **2010**, *132*, 12559 – 12561; b) L. L. Sun, K. E. Hermann, J. Noack, O. Timpe, D. Teschner, M. Hävecker, A. Trunschke, R. Schlögl, *J. Phys. Chem. C* **2014**, *118*, 24611 – 24622; c) Supporting Information; d) P. Schwendt, M. Sivák, A. E. Lapshin, Y. I. Smolin, Y. F. Shepelev, D. Gyepesov, *Transition Met. Chem.* **1994**, *19*, 34 – 36.

[9] a) G. J. Colpas, B. J. Hamstra, J. W. Kampf, V. L. Pecoraro, *J. Am. Chem. Soc.* **1994**, *116*, 3627 – 3628; b) G. J. Colpas, B. J. Hamstra, J. W. Kampf, V. L. Pecoraro, *J. Am. Chem. Soc.* **1996**, *118*, 3469 – 3478.

[10] a) G. Asgedom, A. Sreedhara, C. P. Rao, E. Kolehmainen, *Polyhedron* **1996**, *15*, 3731 – 3739; b) M. R. Maurya, S. Khurana, W. Zhang, D. Rehder, *J. Chem. Soc. Dalton Trans.* **2002**, 3015 – 3023; c) M. R. Maurya, S. Khurana, W. J. Zhang, D. Rehder, *Eur. J. Inorg. Chem.* **2002**, 1749 – 1760; d) M. R. Maurya, *J. Chem. Sci.* **2011**, *123*, 215 – 228; e) M. R. Maurya, N. Chaudhary, F. Avecilla, *Polyhedron* **2014**, *67*, 436 – 448.

[11] D. Rehder, M. Casny, R. Grosse, *Magn. Reson. Chem.* **2004**, *42*, 745 – 749.

[12] C. D. Nunes, P. D. Vaz, V. Felix, L. F. Veiros, T. Moniz, M. Rangel, S. Realista, A. C. Mourato, M. J. Calhorda, *Dalton Trans.* **2015**, *44*, 5125 – 5138.

[13] a) S. Hayashi, K. Hayamizu, *Bull. Chem. Soc. Jpn.* **1990**, *63*, 961 – 963; b) H. Eckert, I. E. Wachs, *J. Phys. Chem.* **1989**, *93*, 6796 – 6805.

[14] a) A. Butler, *Coord. Chem. Rev.* **1999**, *187*, 17 – 35; b) G. Zampella, P. Fantucci, V. L. Pecoraro, L. De Gioia, *Inorg. Chem.* **2006**, *45*, 7133 – 7143.

[15] Z. Cong, S. Yanagisawa, T. Kurahashi, T. Ogura, S. Nakashima, H. Fujii, *J. Am. Chem. Soc.* **2012**, *134*, 20617 – 20620.

[16] a) J. M. Winter, B. S. Moore, *J. Biol. Chem.* **2009**, *284*, 18577 – 18581; b) R. Gupta, G. Hou, R. Renirie, R. Wever, T. Polenova, *J. Am. Chem. Soc.* **2015**, *137*, 5618 – 5628.

[17] a) A. Ansari, P. Jayapal, G. Rajaraman, *Angew. Chem. Int. Ed.* **2015**, *54*, 564 – 568; *Angew. Chem.* **2015**, *127*, 574 – 578; b) A. Yokoyama, J. E. Han, J. Cho, M. Kubo, T. Ogura, M. A. Siegler, K. D. Karlin, W. Nam, *J. Am. Chem. Soc.* **2012**, *134*, 15269 – 15272; c) J. Cho, S. Jeon, S. A. Wilson, L. V. Liu, E. A. Kang, J. J. Braymer, M. H. Lim, B. Hedman, K. O. Hodgson, J. S. Valentine, E. I. Solomon, W. Nam, *Nature* **2011**, *478*, 502 – 505.

[18] a) S. Kozuch, S. Shaik, *Acc. Chem. Res.* **2011**, *44*, 101 – 110; b) D. Usharani, D. Janardanan, C. Li, S. Shaik, *Acc. Chem. Res.* **2013**, *46*, 471 – 482.

[19] a) M. Debnath, A. Dutta, S. Biswas, K. K. Das, H. M. Lee, J. Vãcha, R. Marek, J. Marek, M. Ali, *Polyhedron* **2013**, *63*, 189 – 198; b) P. B. Chatterjee, O. Goncharov-Zapata, L. L. Quinn, G. Hou, H. Hamaed, R. W. Schurko, T. Polenova, D. C. Crans, *Inorg. Chem.* **2011**, *50*, 9794 – 9803; c) O. Goncharova-Zapata, P. B. Chatterjee, G. Hou, L. L. Quinn, M. Li, J. Yehl, D. C. Crans, T. Polenova, *CrystEngComm* **2013**, *15*, 8776 – 8783.

[20] M. P. Waller, M. Bühl, K. R. Geethalakshmi, D. Wang, W. Thiel, *Chem. Eur. J.* **2007**, *13*, 4723 – 4732.

[21] a) M. H. Dickman, M. T. Pope, *Chem. Rev.* **1994**, *94*, 569 – 584; b) D. Maiti, J. S. Woertink, A. A. Narducci Sarjeant, E. I. Solomon, K. D. Karlin, *Inorg. Chem.* **2008**, *47*, 3787 – 3800; c) M. S. Seo, J. Y. Kim, J. Annaraj, Y. Kim, Y.-M. Lee, S.-J. Kim, J. Kim, W. Nam, *Angew. Chem. Int. Ed.* **2007**, *46*, 377 – 380; *Angew. Chem.* **2007**, *119*, 381 – 384.

[22] Gaussian 09, Rev. A.1, M. J. Frisch, G. W. Trucks, H. B. Schlegel, G. E. Scuseria, M. A. Robb, J. R. Cheeseman, G. Scalmani, V. Barone, B. Mennucci, G. A. Petersson, H. Nakatsuji, M. Caricato, X. Li, H. P. Hratchian, A. F. Izmaylov, J. Bloino, G. Zheng, J. L. Sonnenberg, M. Hada, M. Ehara, K. Toyota, R. Fukuda, J. Hasegawa, M. Ishida, T. Nakajima, Y. Honda, O. Kitao, H. Nakai, T. Vreven, J. A. Montgomery Jr., J. E. Peralta, F. Ogliaro, M. J. Bearpark, J. Heyd, E. N. Brothers, K. N. Kudin, V. N. Staroverov, R. Kobayashi, J. Normand, K. Raghavachari, A. P. Rendell, J. C. Burant, S. S. Iyengar, J. Tomasi, M. Cossi, N. Rega, N. J. Millam, M. Klene, J. E. Knox, J. B. Cross, V. Bakken, C. Adamo, J. Jaramillo, R. Gomperts, R. E. Stratmann, O. Yazyev, A. J. Austin, R. Cammi, C. Pomelli, J. W. Ochterski, R. L. Martin, K. Morokuma, V. G. Zakrzewski, G. A. Voth, P. Salvador, J. J. Dannenberg, S. Dapprich, A. D. Daniels, Ö. Farkas, J. B. Foresman, J. V. Ortiz, J. Cioslowski, D. J. Fox, Gaussian, Inc., Wallingford, CT, USA, **2009**.

[23] a) C. T. Lee, W. T. Yang, R. G. Parr, *Phys. Rev. B* **1988**, *37*, 785 – 789; b) A. D. Becke, *J. Chem. Phys.* **1993**, *98*, 5648 – 5652.

[24] a) P. J. Hay, W. R. Wadt, *J. Chem. Phys.* **1985**, *82*, 270 – 283; b) W. R. Wadt, P. J. Hay, *J. Chem. Phys.* **1985**, *82*, 284 – 298.

[25] a) P. J. Hay, W. R. Wadt, *J. Chem. Phys.* **1985**, *82*, 299 – 310; b) R. Ditchfield, W. J. Hehre, J. A. Pople, *J. Chem. Phys.* **1971**, *54*, 724.

[26] a) A. Schäfer, H. Horn, R. Ahlrichs, *J. Chem. Phys.* **1992**, *97*, 2571 – 2577; b) A. Schäfer, C. Huber, R. Ahlrichs, *J. Chem. Phys.* **1994**, *100*, 5829 – 5835.

[27] B. Mennucci, *WIREs Comput. Mol. Sci.* **2012**, *2*, 386 – 404.

[28] G. Schaftenaar, J. H. Noordik, *J. Comput.-Aided Mol. Des.* **2000**, *14*, 123 – 134.

Received: July 11, 2016
Published online on October 18, 2016